Journal of Materials Chemistry A

PAPER

View Article Online
View Journal

Cite this: DOI: 10.1039/c4ta04533e

Hollow Ni–Co–B amorphous alloy nanospheres: facile fabrication *via* vesicle-assisted chemical reduction and their enhanced catalytic performances†

W. Wei, Y. Zhao, S. C. Peng, H. Y. Zhang, Y. P. Bian, H. X. Li and H. Li*

In this paper, we develop a simple vesicle-assisted chemical reduction approach for synthesizing hollow Ni–Co–B nanospheres. With various characterization techniques, the resulting Ni–Co–B nanospheres are identified as amorphous alloys with a hollow chamber. Coexistence of Ni^{II} and Co^{II} species plays a significant role in fabricating hollow nanospheric structures, because only solid nanoparticles can be obtained in the presence of a mono-metallic precursor. During liquid-phase hydrogenation of 2-ethyl-2-hexenaldehyde, hollow Ni–Co–B catalyst displays significant bi-site catalysis from bimetals and delivers much greater activity as well as better selectivity than associated with the dense Ni–Co–B catalyst. Additionally, this catalyst is also easily handled in liquid-phase reactions due to its lower density and magnetic property. The material design concept presented in this work opens a new avenue for the development of hollow non-noble metallic nanospheres and will draw more attention in the foreseeable future.

Received 1st September 2014
Accepted 29th September 2014

DOI: 10.1039/c4ta04533e

www.rsc.org/MaterialsA

Introduction

In recent years, hollow structures have attracted immense attention owing to their potential applications in adsorption, microelectronics, photonics, as well as catalysis.[1] In the domain of catalysis, hollow metallic nanospheres (NSs) with permeable shells represent a new class of efficient catalysts because they offer some advantages over their dense counterparts in terms of increased surface area, low density, easy recovery, self-supporting capacity, cost reduction, and surface permeability.[2] Generally, hollow structures in metals can be routinely fabricated based on a hard templating approach, in which the "hard" templates (*e.g.*, polymer colloid beads and silica spheres) are coated with metallic shell *via* a layer-by-layer technique and then the templates are selectively removed.[2a,b] However, this method is synthetically challenging, since multiple steps are often necessary for achieving hollow metal structures, complicating the preparation process. Strategies based on the mechanisms of galvanic replacement have also been developed to fabricate hollow metal structures,[3] which are more facile and cost-effective since the templates could act as reducing agents to produce metal shells and no additional steps are needed to remove the templates. Nevertheless, the synthesis of hollow metal NSs is limited mainly to noble metals when using this synthesis strategy and thus their practical applications are limited due to the high cost.[4] From the viewpoint of practical applications, exploring more simple approaches to preparing hollow non-noble metal architectures is an important issue.

Recently, attention has turned to developing facile and efficient soft-templating methods for hollow metal structures. Based on a simple vesicle-assisted chemical reduction approach, we successfully synthesized hollow Pd NSs,[2g] which delivered much superior catalytic properties compared to dense Pd nanoparticles (NPs) during liquid-phase phenol hydrogenation. However, the problem resulting from the use of expensive Pd metal has not been completely overcome despite the subsequent synthesis of hollow Pd–Co[2i] and Pd–Fe[2j] NSs through a similar method to economize on the catalyst cost. Therefore, a key issue for the present study is to develop a facile soft-templating method for the synthesis of highly efficient hollow non-noble metallic catalysts.

It is well recognized that a binary alloy is expected to display not only a combination of the properties associated with each of the two distinct metals, but also new capabilities due to a synergistic effect between the two metals.[5] In the case of hydrogenation of 2-ethyl-2-hexenaldehyde (EHEA) to 2-ethyl-1-hexanol

The Education Ministry Key Lab of Resource Chemistry and Shanghai Key Laboratory of Rare Earth Functional Materials, Shanghai Normal University, Shanghai 200234, P. R. China. E-mail: lihui@shnu.edu.cn; Fax: +86 21 6432 2272; Tel: +86 21 6432 3578

† Electronic supplementary information (ESI) available: TEM images of Ni–Co–B-S, Ni–Co–B synthesized by the similar conditions used to synthesize Ni–Co–B-H but without Bu_4PBr, Ni–Co–B synthesized by the similar conditions used to synthesize Ni–Co–B-H but without KCl, and Ni–Co–B-S and Ni–Co–B-H after 5 and 7 consecutive runs, respectively; DSC curves of Ni–Co–B-S and Ni–Co–B-H; UV/vis spectra of aqueous solutions of $NiCl_2$ + $CoCl_2$, $NiCl_2$ + $CoCl_2$ + KCl, and $NiCl_2$ + $CoCl_2$ + KCl + Bu_4PBr; reaction profiles of EHEA hydrogenation over Ni–B, Co–B, and Ni–Co–B-S. See DOI: 10.1039/c4ta04533e

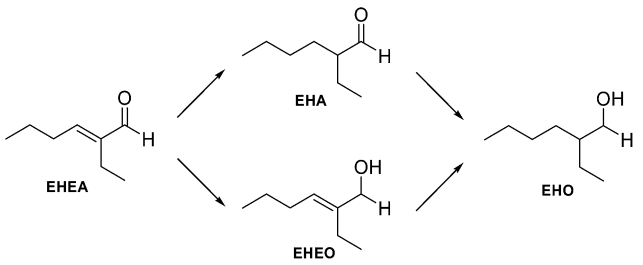

Scheme 1 Possible reaction pathways for EHEA hydrogenation.

(EHO) (Scheme 1), a valuable synthetic alcohol,[6] for instance, highly dispersed Pd on Co–B amorphous alloy displayed significant synergy between sites, in which both metals play specific roles with respect to the reactants.[7] More specifically, Pd prefers the hydrogenation of C=C bonds rather than that of C=O groups in EHEA molecules; while Co is selective to the hydrogenation of C=O bonds and its catalytic activity can be enhanced by a synergetic effect from Pd. Furthermore, Ni is expected to be a possible substitute of Pd for the hydrogenation of C=C bonds because its strong affinity for the adsorption of C=C moieties in α,β-unsaturated aldehydes has been proved in our previous studies.[8] In this research a simple and efficient method to synthesize hollow Ni–Co–B amorphous alloy NSs through a vesicle-assisted chemical reduction method is reported. During the liquid-phase hydrogenation of EHEA to EHO, the hollow Ni–Co–B catalyst displayed much superior performances compared to reference monometallic Ni–B, Co–B, and dense Ni–Co–B catalysts, providing great potential for applications in industry.

Experimental section

Material preparation

All of the chemicals used in this research were of analytical grade and were used without further purification.

Hollow Ni–Co–B amorphous alloy was synthesized by a vesicle-assisted chemical reduction method. In a typical run of catalyst synthesis, an aqueous solution composed of $NiCl_2$ (5.0 mL, 0.10 M) and $CoCl_2$ (5.0 mL, 0.10 M) was first added into an aqueous solution of Bu_4PBr (100 mL, 0.010 M), and then 30 g of KCl was added into the above solution to form a saturated solution. Thereafter, an aqueous solution of KBH_4 (5.0 mL, 0.50 M) was added dropwise under vigorous stirring at 273 K. After the reaction was complete, the black precipitate was washed free from inorganic ions and soluble amphiphilic substances with deionized water until pH $\sim$ 7 was achieved, followed by three washings with absolute alcohol (EtOH). Finally, the sample was stored in EtOH until use. The as-prepared hollow Ni–Co–B amorphous alloy was designated Ni–Co–B-H (hollow). The Ni and Co contents in the Ni–Co samples were adjusted by varying the molar ratio of Ni^{2+}/Co^{2+} in the precursor solution. Without addition of Co^{2+} or Ni^{2+} in the preparation solution, pure Ni or Co was also synthesized. For comparison, a solid Ni–Co–B amorphous alloy was also prepared by the conventional method, that is, by direct reduction of Ni^{2+} and Co^{2+} with KBH_4, which was denoted as Ni–Co–B-S (solid).

Material characterization

The bulk composition was analyzed by means of inductively coupled plasma optical emission spectrometry (ICP-OES; Varian VISTA-MPX). The amorphous structure was investigated by both X-ray diffraction (XRD; Rigaku D/Max-RB with Cu Kα radiation) and selective-area electronic diffraction (SAED; JEOL JEM2100). The crystallization process was followed by differential scanning calorimetry (DSC; Shimadzu DSC-60) under an N_2 atmosphere at a heating rate of 5 K min^{-1}. The shapes and morphologies of catalysts were observed by both field emission scanning electron microscopy (FESEM; Hitachi S-4800) and transmission electron microscopy (TEM; JEOL JEM2100). The surface electronic states were determined by X-ray photoelectron spectroscopy (XPS; ULVAC-PHI PHI5000 VersaProbe system using Al Kα radiation), during which all samples were pretreated *in situ* in a pure Ar atmosphere to avoid oxidation. The binding energy (BE) values were calibrated by using C 1s = 284.6 eV as a reference. The active surface area (S_{act}) was measured by hydrogen chemisorption with a Micromeritics AutoChem II 2920 instrument assuming H/M(s) = 1 and a surface area of 6.5×10^{-20} m^2 per M atom. The hydrogen temperature-programmed desorption (H_2-TPD) curve was obtained with the same instrument in Ar flow at a ramping rate of 10 K min^{-1}.

Activity test

In a typical experiment, liquid-phase hydrogenation of 2-ethyl-2-hexenaldehyde was carried out in a 250 mL stainless steel autoclave containing 0.3 g Ni–Co–B-H, 4 mL of 2-ethyl-2-hexenaldehyde, 45 mL of EtOH, and 1.0 MPa of H_2 at 373 K. The reaction mixture was sampled at intervals for product analysis using a gas chromatograph equipped with an EC-WAX column and a flame ionization detector. All results have been reproduced and the error was limited to within 5%. Preliminary kinetic studies revealed the following: that there was a plateau in the dependency of the reaction initial rate when the stirring rate was above 750 rpm; and that the reaction initial rate varied linearly with the catalyst amount from 0.1 to 0.5 g, indicating that the stirring rate of 800 rpm was high enough such that the hydrogenation rates were independent of mass transfer. After cooling to room temperature at the end of the reaction, the catalyst was separated by a magnet and washed with deionized water and EtOH for further characterization and applications. To test the catalyst durability, the used catalyst was separated and washed thoroughly with deionized water and EtOH after each run of the reaction. Then, the catalyst was reused with a fresh charge of substances for a subsequent recycle run under the same reaction conditions.

Results and discussion

Structural characteristics

Ni–Co–B-H was first synthesized in an aqueous solution by using a $Bu_4P^+/[MX_4]^{2-}$ (M = Ni and Co) composite vesicle stemming from the strong electrostatic interaction between Bu_4P^+ and $[MX_4]^{2-}$ as precursors and structure-directing

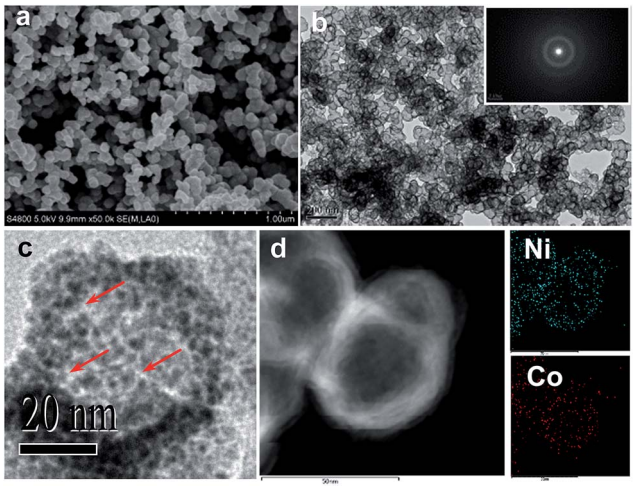

Fig. 1 (a) FESEM and (b) TEM images of Ni–Co–B-H. (c) TEM image of a single Ni–Co–B-H hollow sphere. (d) EDS mapping of one sphere in (b). The inset is the SAED pattern.

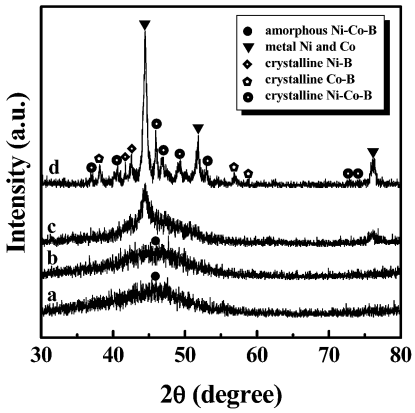

Fig. 2 XRD patterns of (a) the fresh Ni–Co–B-H, (b) the fresh Ni–Co–B-S, and (c) the Ni–Co–B-H and (d) the Ni–Co–B-S after being treated at 673 K for 2 h in N_2 flow.

Table 1 Structural parameters of the as-prepared catalysts

Catalyst	Bulk composition (atom%)	Surface composition (atom%)	S_{Pt} (m^2 g^{-1})
Ni–Co–B-S	$Ni_{34}Co_{33}B_{33}$	$Ni_{41}Co_{30}B_{29}$	16
Ni–Co–B-H	$Ni_{31}Co_{31}B_{38}$	$Ni_{39}Co_{28}B_{33}$	30

template. The FESEM image in Fig. 1a reveals that Ni–Co–B-H displays uniform spheres with an average diameter around 40 nm. Meanwhile, the TEM observation of Ni–Co–B-H (Fig. 1b) shows clear contrast difference between the center and the edge, indicating the interior of these NSs is hollow. The high-magnification TEM image of an individual sphere (Fig. 1c) reveals that the outer shell of Ni–Co–B-H is comprised of uniform particles with an average size of 2 nm. These NPs constitute a self-supported shell with wormhole-like mesopores (marked with arrows), which should provide a pathway for high diffusion. The pore size is roughly estimated to be about 2 nm. The energy-dispersive spectrometry (EDS) mapping for a single Ni–Co–B-H sphere (Fig. 1d) shows the distribution of Ni and Co is very uniform throughout the whole shell of hollow NS. In contrast to the hollow NSs, the Ni–Co–B (Fig. 1S†) obtained *via* the conventional method in pure aqueous solution is present in the form of solid NPs with extremely broad size distribution (Ni–Co–B-S).

The inset SAED image in Fig. 1b displays successive diffraction halos indicative of a typical amorphous structure.[9] Furthermore, XRD patterns (Fig. 2) demonstrate that, similar to the conventional Ni–Co–B-S, the fresh Ni–Co–B-H is present as a typical amorphous structure indicated by a single broad peak around $2\theta = 45°$.[10] Heat treatment of the fresh Ni–Co–B samples (at 673 K in N_2 for 2 h) resulted in the appearance of several diffraction peaks corresponding to metallic Ni and Co, and crystalline Ni–B, Co–B and Ni–Co–B alloys. The appearance of Ni–Co–B crystalline phases during the crystallization process verified the formation of alloys between Ni, Co and B for the as-prepared Ni–Co–B, as demonstrated by our previous studies.[11] The heat-treated Ni–Co–B-H exhibited fewer crystalline phases relative to the heat-treated Ni–Co–B-S, indicating the stronger thermal stability against crystallization. This might be related to the increased B content in Ni–Co–B-H compared to Ni–Co–B-S,[12] as demonstrated by ICP-OES analysis (Table 1). The crystallization process was further investigated by DSC analysis. As shown in Fig. S2,† Ni–Co–B-H exhibits an exothermic peak at 740 K higher by at least 57 K than that for Ni–Co–B-S, further confirming the enhanced thermal stability of the former. XPS reveals that for all the Ni species in either Ni–Co–B-S or Ni–Co–B-H, the core level of Ni $2p_{3/2}$ is at 852.7 eV (Fig. 3), indicating that all Ni atoms are present in the metallic state.[11,13] Meanwhile, only one peak with BE at *ca.* 778.2 eV is observed in the Co $2p_{3/2}$ level, indicating that almost all the Co species are present as the metallic state in both samples.[11,14] However, the B species are present as both elemental B and oxidized B, with B 1s BE values of around 188.1 and 192.9 eV. The B 1s BE of elemental B in either Ni–Co–B-S or Ni–Co–B-H exceeds that of pure B (187.1 eV)[13] by 1.0 eV, further proving that the elemental B is alloyed with the metallic Ni or Co. In alloys, partial electrons may be transferred from B to Ni or Co, as well demonstrated previously.[11,13] Thus, the combined results from SAED, XRD,

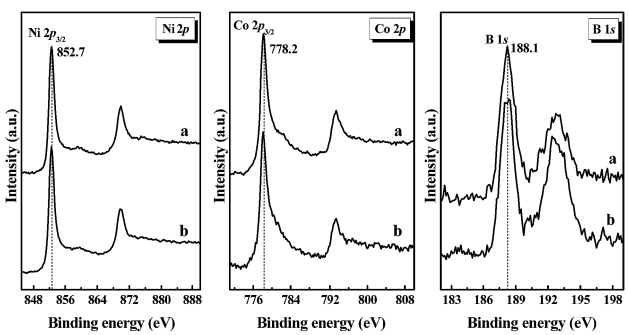

Fig. 3 XPS spectra of (a) Ni–Co–B-S and (b) Ni–Co–B-H.

DSC, and XPS characterizations clearly demonstrated the formation of Ni–Co–B amorphous alloy through the present preparation method. According to the calculation based on XPS peak areas, the surface molar ratio of the alloying B to the metallic Ni and Co (Table 1) in Ni–Co–B-H is 33/67, higher than that in Ni–Co–B-S (29/71), implying that the present preparation method has significant influence on the surface composition of Ni–Co–B amorphous alloy, and Ni–Co–B-H is surface-enriched with the alloying B relative to Ni–Co–B-S.

Formation process

The formation of hollow Ni–Co–B NSs is likely based on the $Bu_4P^+/[MX_4]^{2-}$ (M = Ni and Co) composite vesicles, which provide templates for the growth of hollow structures. The vesicle-assisted chemical reduction process might consist of two steps (Scheme 2). The first step should be the formation of spherical vesicle precursors induced by the electrostatic interaction between $[MX_4]^{2-}$ and Bu_4P^+. The KCl and the Bu_4PBr in water may be dissociated and provide Cl^- and Br^- ions. These halide anions can coordinate with M^{2+} (M = Ni and Co) to form $[MX_4]^{2-}$. The coordination of X^- to M^{2+} was evidenced by the distinct red shift of the UV/visible absorption (Fig. S3†). The strong electrostatic interaction between Bu_4P^+ and $[MX_4]^{2-}$ induces the rapid co-assembly into $Bu_4P^+/[MX_4]^{2-}$ composite vesicles. The formation of vesicles has been confirmed by the TEM image (Fig. 4), which displays almost the same diameter (45 nm) as the average interior-cavity size of the final product (see Fig. 1). The second step is the reduction of the confined $[MX_4]^{2-}$ ions with borohydride into Ni–Co–B clusters, which grow to particles coating the vesicles and constructing a thin shell surrounding the vesicle templates. After removing the vesicle template by washing with water, hollow Ni–Co–B NSs are obtained. The wormhole-like mesoporous structure of the outer shell can be attributed to the pileup of Ni–Co–B NPs.

Both Bu_4PBr and KCl play a key role in fabricating hollow Ni–Co–B NSs. Only solid Ni–Co–B NPs with a broad size range were obtained without using the Bu_4PBr template (Fig. S4†). Because the coordination of Br^- with M^{2+} is not strong enough to induce a reaction between $[MBr_4]^{2-}$ and BH_4^- to occur in a smooth manner, the strongly exothermic reaction leads to the formation of irregular Ni–Co–B particles in the absence of KCl while keeping other experimental conditions the same as those of the typical preparation (Fig. S5†).

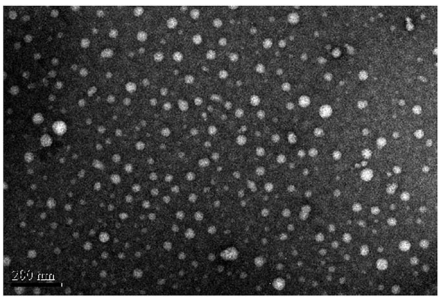

Fig. 4 TEM image of vesicles formed through a mixture of $NiCl_2$/$CoCl_2$/KCl/Bu_4PBr obtained by drop-depositing solutions on carbon grids and staining with phosphotungstanic acid.

Furthermore, the Ni/Co molar ratio also significantly influences the formation of hollow NSs. We point out that neither hollow Ni–B nor hollow Co–B (ref. 14) was formed if monometallic precursor was used (Fig. 5). Meanwhile, Zhang and Li[15] had demonstrated that $CoCl_2$ does not induce vesicle formation in the presence of Bu_4NBr. More interestingly, co-reduction of mixed $[NiX_4]^{2-}$ and $[CoX_4]^{2-}$ with Ni/Co molar ratio of 1/1 appears to form hollow NSs in high yield (see Fig. 1b). Increasing the Ni/Co molar ratio to 3/1 or decreasing it to 1/3 led to the formation of a mixture of hollow and solid particles (Fig. 6a and b). Almost solely solid samples were obtained with further increasing or decreasing the Ni/Co molar ratio to 5/1 or 1/5 (Fig. 6c and d). Based on these results, we propose that the formation of the hollow Ni–Co–B NSs is originated from the co-reduction of $[NiX_4]^{2-}$ and $[CoX_4]^{2-}$ confined on the surface of vesicles and the subsequent growth into a thin shell coating the vesicles. Accordingly, the generation of $[MX_4]^{2-}$ complexes has both positive and negative influences on the fabrication of hollow NSs. On the one hand, the strong electrostatic interaction between Bu_4P^+ and $[MX_4]^{2-}$ can induce the formation of $Bu_4P^+/[MX_4]^{2-}$ composite vesicles, providing a structure-directing template. On the other hand, the generation of $[MX_4]^{2-}$ complexes is expected to decrease the reducibility of M^{II} species. Therefore, slower reduction of $[NiX_4]^{2-}$ or $[CoX_4]^{2-}$ allows the vesicle phase to reorganize, and only large particles to grow (Fig. 5). Indeed, the chemical preparation of M–B amorphous alloy is an autocatalytic reaction, *i.e.*, the formation of M–B can be catalyzed by itself.[16] Extended X-ray absorption fine

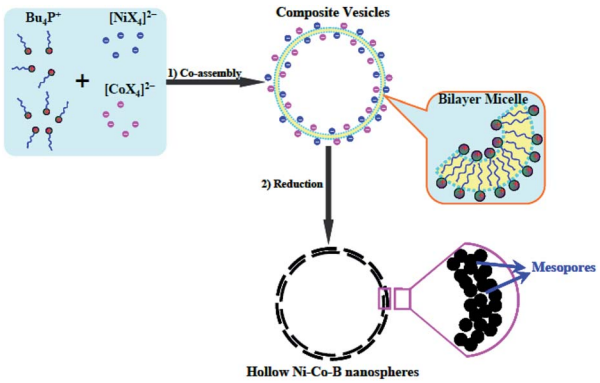

Scheme 2 Illustration of the formation process of hollow Ni–Co–B nanospheres.

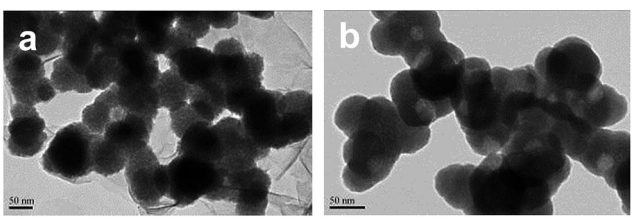

Fig. 5 TEM images of (a) Ni–B and (b) Co–B synthesized under the same conditions used to synthesize Ni–Co–B-H.

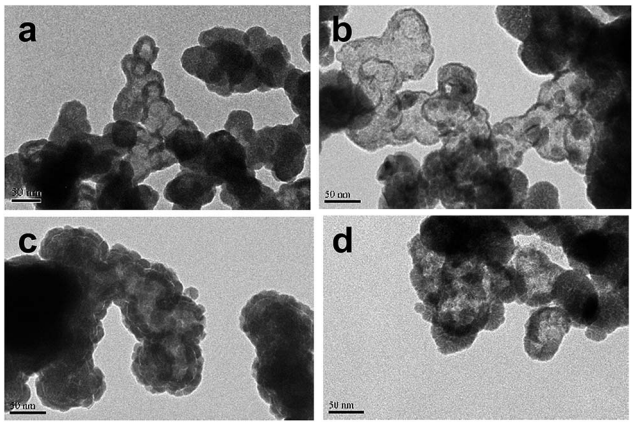

Fig. 6 TEM images of Ni–Co–B synthesized under the same conditions used to synthesize Ni–Co–B-H but with different Ni/Co molar ratios: (a) Ni/Co = 3/1, (b) Ni/Co = 1/3, (c) Ni/Co = 5/1, (d) Ni/Co = 1/5.

structure (EXAFS) analysis revealed that Ni and Co have a synergistic effect to the structure of the bimetallic Ni–Co–B amorphous alloys.[17] Specifically, co-existence of Ni and Co strengthens the M–B interaction and increases the structural disordering factors of Ni–Co–B. The effect of Co content in Ni–Co–B on these parameters is represented in a volcano-shaped curve, and the maximum values are achieved for Ni/Co molar ratio of 1/1. As a result, co-reduction of a mixture containing the same amount of $[NiX_4]^{2-}$ and $[CoX_4]^{2-}$ affords highly active primary Ni–Co–B particles at the interface of vesicles. Subsequently, these primary particles agglomerate and coalesce quickly, until a wall thickness is reached at which the structure is mechanically stable. Besides the molar ratio of $[NiX_4]^{2-}$ to $[CoX_4]^{2-}$, both the concentration of borohydride aqueous solution and the reduction temperature are also important for obtaining well-defined hollow structured Ni–Co–B. As confirmed by TEM images (Fig. 7), co-reduction of the mixed $[NiX_4]^{2-}$ and $[CoX_4]^{2-}$ with low concentration of borohydride (0.05 M) could not achieve evident hollow structures. It is noteworthy that much lower reduction temperature (263 K) produces completely dense particles. Accordingly, the inability to achieve hollow structures should be due to the reduction rate being too slow to form an integrated outer shell covering the vesicles. The proposed mechanism can also explain why only fast reduction is able to generate such a hollow metallic nanostructure; only then can the hollow nanoarchitecture be generated before the vesicle phase is able to rearrange.

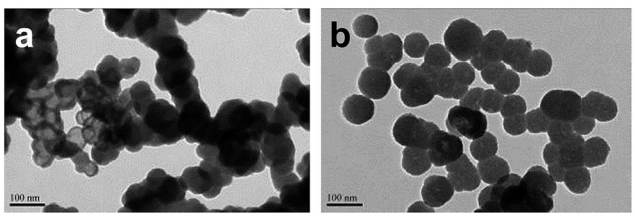

Fig. 7 TEM images of Ni–Co–B synthesized under the same conditions used to synthesize Ni–Co–B-H but (a) with low concentration (0.05 M) or (b) at low reduction temperature (263 K).

Catalytic performances

The hollow chambers of Ni–Co–B-H are very stable, and can be well preserved in water for several months. Additionally, the shells of this material are thin (~3 nm) and porous, which is expected to have little influence on the diffusion of reaction molecules in liquid-phase reaction. More importantly, these hollow NSs can be readily dispersed in liquid-phase solution due to their low density, and can be easily recovered from a reaction system by a magnet due to their magnetic property (Fig. 8). All these properties present opportunities for this material to be used as a highly efficient catalyst in liquid-phase reaction. The as-prepared catalysts were subjected to liquid-phase EHEA hydrogenation to EHO for evaluating their performances. In addition to the production of target product (EHO), both 2-ethylhexanal (EHA) and 2-ethyl-2-hexenol (EHEO) were identified as by-products (Scheme 1) under the present conditions, 1.0 MPa of H_2 and 373 K.

Preliminary studies suggested that Ni–B prefers the hydrogenation of C=C bonds rather than that of C=O bonds in EHEA molecules (Fig. S6a†) due to its strong affinity for the adsorption of the C=C group;[8] while Co–B exhibits nearly the same initial selectivity to EHO as to EHA, giving equivalent chances for both C=O and C=C hydrogenation (Fig. S6b†). Thanks to the synergistic effect of Ni and Co demonstrated by EXAFS analysis,[17] binary-metallic Ni–Co–B-S amorphous alloy delivered much higher catalytic activity and selectivity (Fig. S6c†) than the mono-metal amorphous alloys. Although EHO can be obtained with high yield (>90%) over Ni–Co–B-S, saturated aldehyde (EHA) could not be hydrogenated completely to the final product under the present conditions. Compared with Ni–Co–B-S, Ni–Co–B-H displayed similar bi-site catalysis from bimetals and evidently much improved catalytic activity (Fig. 9a). The higher catalytic activity of Ni–Co–B-H can be mainly attributed to its larger number of active sites (see Table 1), deriving from the hollow structures with mesopores. More specifically, the mesopores are large enough to allow the penetration of substances and it is possible for the catalytic reaction to occur on the inner side of the shell. On the other hand, the increased hydrogenation ability for C=O bonds associated with Ni–Co–B-H (see Fig. S6c† and 9a) can be partially due to its higher surface B content relative to Ni–Co–B-S as confirmed by XPS. It is well documented that surface B-enrichment results in higher

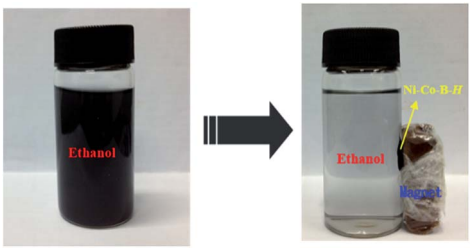

Fig. 8 Illustration of the easy handling of Ni–Co–B-H catalyst in liquid-phase reaction.

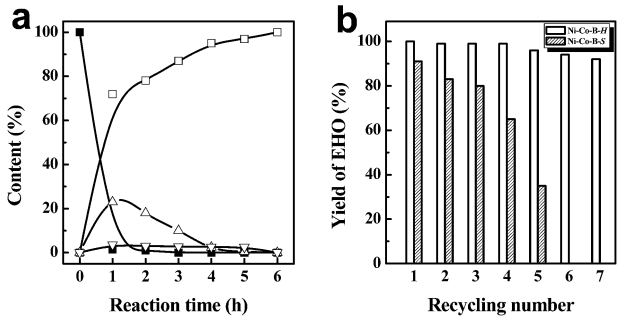

Fig. 9 (a) Reaction profile and (b) recycling test of EHEA hydrogenation over Ni–Co–B-H. (■) EHEA, (□) EHO, (△) EHA, and (▽) EHEO. Reaction conditions: catalyst (0.3 g), EHEA (4 mL), EtOH (45 mL), T = 373 K, P_{H_2} = 1.0 MPa, stirring rate = 800 rpm. Each run was conducted for 6 h in the recycling test.

electron density on metal active sites in M–B amorphous alloys,[12,14] which is favorable for the formation of H^- species[18] and activation of the adsorbed C=O groups through an electron back-donation from the $d_{x^2-y^2}$ orbital of metal to the $\pi^*_{C=O}$ antibonding orbital of the C=O bonds,[19] leading to the enhanced reactivity.

Besides its high efficiency, Ni–Co–B-H could be easily separated from the reaction solution by a magnet and used repeatedly for more than 7 times with only 7% decrease of EHO yield in EHEA hydrogenation (Fig. 9b). However, the EHO yield decreases by 62% over Ni–Co–B-S after being used 5 times. ICP analysis revealed that the weight loss of Ni–Co–B-S after 5 consecutive runs is 27%, while no leaching of Ni or Co could be detected for Ni–Co–B-H during repeated use. This implies that the larger diameter of hollow NSs can reduce the loss of catalyst during recycling tests. Additionally, TEM images (Fig. S7†) reveal that the deactivation of Ni–Co–B-S can also be due to a severe agglomeration of NPs. However, the hollow chambers of Ni–Co–B-H are quite stable which can be well preserved after being used 7 times. According to this observation, the high durability of Ni–Co–B-H can also be attributed to its self-supporting capacity, which retards the Ni–Co–B NPs from agglomeration during the hydrogenation process.

Conclusions

In summary, we developed a simple approach for synthesizing hollow-structured Ni–Co–B amorphous alloy NSs. Based on various characterizations, a vesicle-assisted chemical reduction mechanism to form such a hollow structure is proposed. In particular, our present method is facile and cost-effective. Thus, this strategy can potentially be extended to other hollow metallic NSs with different composition. The one-pot production of EHO through EHEA hydrogenation highlights the role of the significant bi-site catalysis from bimetals. This might provide a preferable method for the synthesis of other hollow multi-metallic catalysts and offer new levels of control of catalytic properties.

Acknowledgements

This work was supported by the National Natural Science Foundation of China (21273149), PCSIRT (IRT1269), the Program for New Century Excellent Talents in University (NCET-11-1052), and the Shanghai Science & Technology and Education Committee (11JC1408900, 12490502800, 10SG41, 12YZ084).

Notes and references

1 (*a*) Y. Sun, B. Mayers and Y. Xia, *Adv. Mater.*, 2003, **15**, 641; (*b*) Y. Song, R. M. Garcia, R. M. Dorin, H. Wang, Y. Qiu and J. A. Shelnutt, *Angew. Chem., Int. Ed.*, 2006, **45**, 8126; (*c*) H. X. Li, Z. F. Bian, J. Zhu, D. Q. Zhang, G. S. Li, Y. N. Huo, H. Li and Y. F. Lu, *J. Am. Chem. Soc.*, 2007, **129**, 8406; (*d*) H. Xu and W. Wang, *Angew. Chem., Int. Ed.*, 2007, **46**, 1489.

2 (*a*) S. W. Kim, M. Kim, W. Y. Lee and T. Hyeon, *J. Am. Chem. Soc.*, 2002, **124**, 7642; (*b*) X. Chen, W. Yang, S. Wang, M. Qiao, S. Yan, K. Fan and H. He, *New J. Chem.*, 2005, **29**, 266; (*c*) Y. Li, P. Zhou, Z. Dai, Z. Hu, P. Sun and J. C. Bao, *New J. Chem.*, 2006, **30**, 832; (*d*) P. Zhou, Y. Li, P. Sun, J. Zhou and J. C. Bao, *Chem. Commun.*, 2007, 1418; (*e*) G. Chen, D. Xia, Z. Nie, Z. Wang, L. Wang, L. Zhang and J. Zhang, *Chem. Mater.*, 2007, **19**, 1840; (*f*) F. Cheng, H. Ma, Y. Li and J. Chen, *Inorg. Chem.*, 2007, **46**, 788; (*g*) H. Li, J. Liu, S. Xie, M. Qiao, W. Dai, Y. Lu and H. X. Li, *Adv. Funct. Mater.*, 2008, **18**, 3235; (*h*) H. Li, Y. Xu, J. Liu, Q. F. Zhao and H. X. Li, *J. Colloid Interface Sci.*, 2009, **334**, 176; (*i*) H. Li, Z. H. Zhu, J. Liu, S. H. Xie and H. X. Li, *J. Mater. Chem.*, 2010, **20**, 4366; (*j*) H. Li, Z. H. Zhu, H. X. Li, P. Li and X. G. Zhou, *J. Colloid Interface Sci.*, 2010, **349**, 613; (*k*) H. Li, D. Q. Zhang, G. S. Li, Y. Xu, Y. F. Lu and H. X. Li, *Chem. Commun.*, 2010, **46**, 791; (*l*) H. Li, H. Lin, Y. Hu, H. X. Li, P. Li and X. G. Zhou, *J. Mater. Chem.*, 2011, **21**, 18447.

3 Y. Sun and Y. Xia, *Science*, 2002, **298**, 2176.

4 (*a*) Y. Sun, B. T. Mayers and Y. Xia, *Nano Lett.*, 2002, **2**, 481; (*b*) H. P. Liang, H. M. Zhang, J. S. Hu, Y. G. Guo, L. J. Wan and C. L. Bai, *Angew. Chem., Int. Ed.*, 2004, **43**, 1540; (*c*) H. P. Liang, Y. G. Guo, H. M. Zhang, J. S. Hu, L. J. Wan and C. L. Bai, *Chem. Commun.*, 2004, 1496; (*d*) H. P. Liang, L. J. Wan, C. L. Bai and L. Jiang, *J. Phys. Chem. B*, 2005, **109**, 7795.

5 R. Ferrando, J. Jellinek and R. L. Johnston, *Chem. Rev.*, 2008, **108**, 845.

6 I. Kirshenbaum and E. J. Inchalik, in *Kirk-Othmer Encyclopedia of Chemical Technology*, ed. M. Grayson and D. Eckroth, John Wiley & Sons, New York, 3rd edn, 1981, vol. 16, pp. 637–653.

7 J. Q. Ma, L. Xu, L. Xu, H. Wang, S. Xu, H. X. Li, S. H. Xie and H. Li, *ACS Catal.*, 2013, **3**, 985.

8 H. X. Li, X. F. Chen, M. H. Qiao and Y. P. Xu, *Appl. Catal., A*, 2002, **225**, 117.

9 K. S. Martens, J. A. Parton, R. Vercruysse, K. Jacobs and P. A. Maier, *Catal. Lett.*, 1996, **38**, 209.

10 A. Yokoyama, H. Komiyama, H. Inoue, T. Masumoto and H. M. Kimura, *J. Catal.*, 1981, **68**, 355.

11 H. X. Li, Y. D. Wu, J. Zhang, W. L. Dai and M. H. Qiao, *Appl. Catal., A*, 2004, **275**, 199.
12 H. X. Li, H. Li, W. L. Dai and M. H. Qiao, *Appl. Catal., A*, 2003, **238**, 119.
13 H. Li, H. X. Li, W. L. Dai, W. J. Wang, Z. G. Fang and J. F. Deng, *Appl. Surf. Sci.*, 1999, **152**, 25.
14 Z. H. Zhu, J. Q. Ma, L. Xu, L. Xu, H. X. Li and H. Li, *ACS Catal.*, 2012, **2**, 2119.
15 X. J. Zhang and D. Li, *Angew. Chem., Int. Ed.*, 2006, **45**, 5971.
16 Y. Chen, *Catal. Today*, 1998, **44**, 3.
17 B. R. Shen, S. Q. Wei, K. N. Fan and J. F. Deng, *Appl. Phys. A*, 1997, **65**, 295.
18 H. Noller and W. M. Lin, *J. Catal.*, 1984, **85**, 25.
19 E. Boellaard, R. J. Vreeburg, O. L. J. Gijzeman and J. W. Geus, *J. Mol. Catal.*, 1994, **92**, 299.